Journal of Biomechanics ∎ (∎∎∎∎) ∎∎∎–∎∎∎

Contents lists available at ScienceDirect

Journal of Biomechanics

journal homepage: www.elsevier.com/locate/jbiomech
www.JBiomech.com

Cardiac MRI based numerical modeling of left ventricular fluid dynamics with mitral valve incorporated

Boyang Su [a], Ru San Tan [a,b], Ju Le Tan [a], Kenneth Wei Qiang Guo [a], Jun Mei Zhang [a,b], Shuang Leng [a], Xiaodan Zhao [a], John Carson Allen [b], Liang Zhong [a,b,*]

[a] National Heart Centre Singapore, 5 Hospital Drive, 169609, Singapore
[b] Duke-NUS Graduate Medical School Singapore, Singapore

ARTICLE INFO

Article history:
Accepted 3 March 2016

Keywords:
Computational fluid dynamics
Bileaflet mitral valve
Vortex formation
Patient-specific

ABSTRACT

Recent numerical studies were focused on the modeling of flow in patient-specific left ventricle (LV); however, the mitral valve (MV) was usually excluded. In this study, both patient-specific LV and MV were modeled to achieve a more realistic intraventricular flow. Cardiac MRI images were acquired from a pulmonary arterial hypertension (PAH) patient and a healthy volunteer, and manual segmentation was conducted to reconstruct three-dimensional (3D) LV and MV geometries at each frame. Based on these 3D geometries, vortex formation time (VFT) was derived, and the values were 4.0 and 6.5 for the normal subject and the PAH patient, respectively. Based on studies in the literature, VTF in the healthy subject fell within the normal range, while that in the PAH patient exceeded the threshold for normality. The vortex structures in the LV clearly showed that the vortex ring was initiated from the tips of the MV instead of the mitral annulus. The excessive VFT during the rapid filling phase in the PAH patient resulted in a trailing flow structure behind the primary vortex ring, which was not observed in the normal subject. It can be deduced from this study that incorporating the MV into a patient-specific model is necessary to produce more reasonable VFT and intraventricular flow.

1. Introduction

Despite numerous studies of blood flow in the left ventricle (LV) (Pedrizzetti and Domenichini, 2014), the association between the LV flow structure and the cardiac remodeling is still not well understood. Various approaches have been applied to visualize the flow structure in the LV such as echocardiography and cardiac magnetic resonance (CMR) (Charonko et al., 2013; Garcia et al., 2010; Rodriguez Muñoz et al., 2013). Besides *in-vivo* studies, extensive *in-vitro* studies have been conducted to measure the intraventricular flow using a heart simulator (Falahatpisheh and Kheradvar, 2012; Kheradvar and Gharib, 2007). Owing to the difficulties in mimicking a native heart ventricle, the primary purpose of *in-vitro* studies is to understand the fluid dynamics in an idealized heart ventricle. Computational fluid dynamics (CFD) in conjunction with CMR is emerging as an alternative tool to further facilitate the visualization of patient-specific LV flow, as it is capable of providing a more detailed flow structure with much higher resolutions (Chnafa et al., 2014; Mangual et al., 2013; Saber et al., 2003; Schenkel et al., 2009; Su et al., 2014a).

As an asymmetric bileaflet mitral valve (MV) is located at the inflow tract of the LV, it has been shown that incorporation of the MV into the numerical model will give more realistic flow field predictions (Domenichini and Pedrizzetti, 2014; Seo et al., 2014; Votta et al., 2013). However, the MV was only modeled in very limited numerical simulations, due to the difficulties in reconstructing and modeling the dynamic MV. In the studies focusing on the mitral leaflets, the MV was scanned using real-time 3D transesophageal echocardiography (TEE) (Chandran and Kim, 2014). To obtain better accuracy such as papillary muscles and chordae, CMR was also adopted to scan a number of evenly rotated long-axis planes (Dimasi et al., 2012; Stevanella et al., 2011). It is worth noting that this method was not routinely used in clinical CMR imaging. A few studies used high spatial resolution of Computed Tomography (CT) images to reconstruct the MV and LV to study the intraventricular flow (Chnafa et al., 2014, 2012). Its usage is limited by the complications of ionizing radiation and relatively low temporal resolution. Routine clinical CMR scanning (*i.e.* two-chamber, three-chamber, four-chamber and short-axis planes) is able to provide adequate information to reconstruct a patient-specific LV. Nevertheless, it is difficult to segment mitral leaflet in

* Corresponding author at: National Heart Centre Singapore, 5 Hospital Drive, 169609, Singapore. Tel.: +65 67042237; fax: +65 62230972.
E-mail address: zhong.liang@nhcs.com.sg (L. Zhong).

http://dx.doi.org/10.1016/j.jbiomech.2016.03.008
0021-9290/

all views, and a generic one defined by mathematical equations is a feasible approach (Domenichini and Pedrizzetti, 2014).

In the literature, most LV numerical simulations focused on understanding the LV fluid dynamics in normal subjects, while limited studies modeled the patient-specific LVs with heart failure, dilated cardiomyopathy, and hypertrophic cardiomyopathy (Khalafvand et al., 2014; Mangual et al., 2013; Su et al., 2014a). These studies have demonstrated that the structure of vortices is different in normal cases compared to patient cases. To the best of our knowledge, no numerical study of LV flow has been conducted in pulmonary arterial hypertension (PAH) patients. In addition, these patient-specific studies ignored the influence of MV, which impaired the reliability of the numerical results to a certain extent. In this study, CMR images acquired from a normal subject and a PAH patient were selected for MV and LV reconstructions and the following numerical simulations. Geometrical parameters (*e.g.* ventricular volume and vortex formation time (VFT)) and the detailed fluid structures in these two models were analyzed to observe the impact of PAH. In addition, the study outlined a framework for more realistic LV flow based CMR images.

2. Methods

2.1. Data acquisition

One healthy volunteer and one PAH patient were recruited in this study, and CMR scans were carried out on a Philips 3.0 T system (Ingenia, Philips Healthcare, Netherlands) with a dStream Torso coil (maximum number of channels 32). BTFE end-expiratory breath hold cine images were acquired in multi-planar views (namely two-chamber, three-chamber, four-chamber, short-axis views as indicated in Fig. 1). Electrocardiographically (ECG) gated consecutive cine short-axis images were acquired from apex to mid-atrium (8 mm slice thickness with 2 mm interslice gap). The acquisition included 12–14 short-axis slices covering the entire LV and partial aorta and atrium. Note that the acquisition rates of long-axis and short-axis images were 40 and 30 frames per cardiac cycle, respectively.

2.2. Geometry reconstruction

The study was focused on the LV flow and thus the inlet and outlet of the LV chamber were mitral and aortic valves, respectively. In addition to the MV and LV, the left atrium was partially reconstructed to minimize the influences of the inlet boundary condition on the intraventricular flow. Manual segmentation was performed to extract the inner layer on myocardium (endocardium) over the entire cardiac cycle as indicated in Fig. 1. Spatial information (*e.g.* resolution, spacing and orientation) stored in Digital Imaging and COmmunications in Medicine (DICOM) image allowed CMR images to be assembled in three-dimension (3D) as well as 3D contours (Fig. 2A). The large spacing short-axis images could not be used to identify mitral annulus, and six vertices selected from the long-axis images were utilized for its reconstruction instead (Fig. 2A). In addition, the ventricular annulus, which enclosed both mitral and aortic orifices was reconstructed

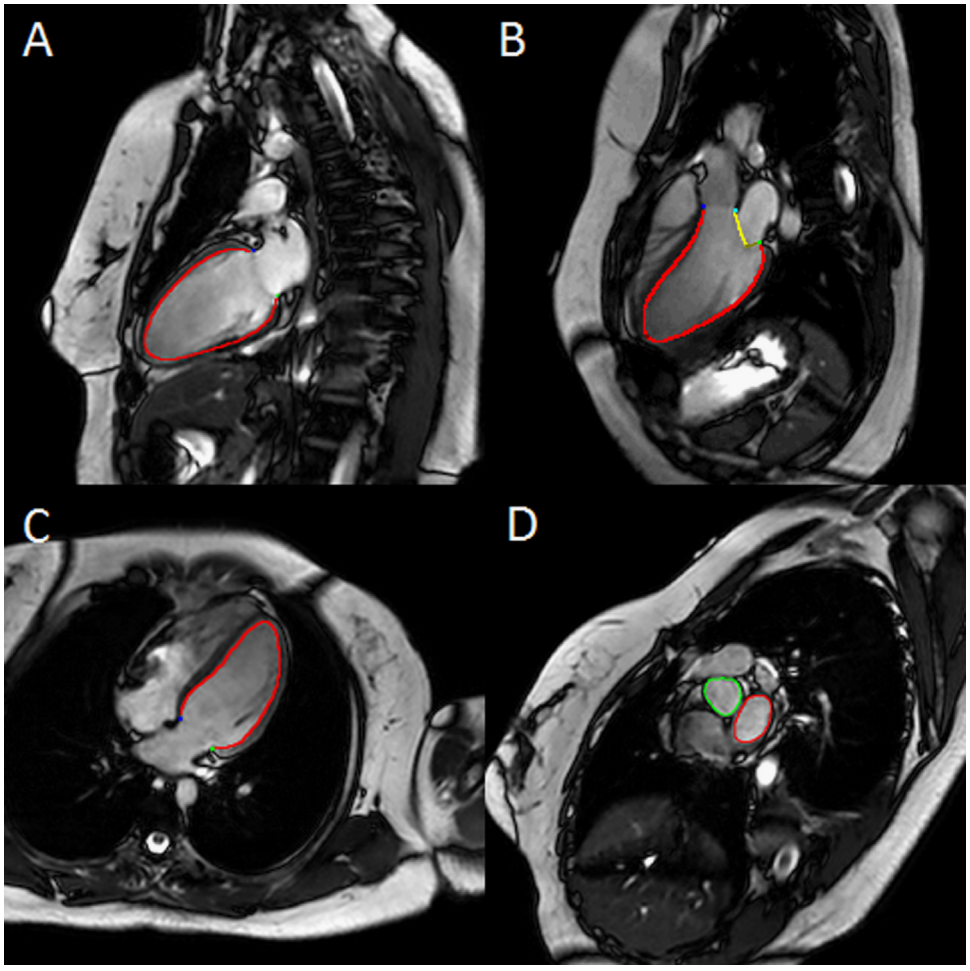

Fig. 1. CMR images: (A) two-chamber view, (B) three-chamber view, (C) four-chamber view and (D) Short-axis view.

Please cite this article as: Su, B., et al., Cardiac MRI based numerical modeling of left ventricular fluid dynamics with mitral valve incorporated. Journal of Biomechanics (2016), http://dx.doi.org/10.1016/j.jbiomech.2016.03.008

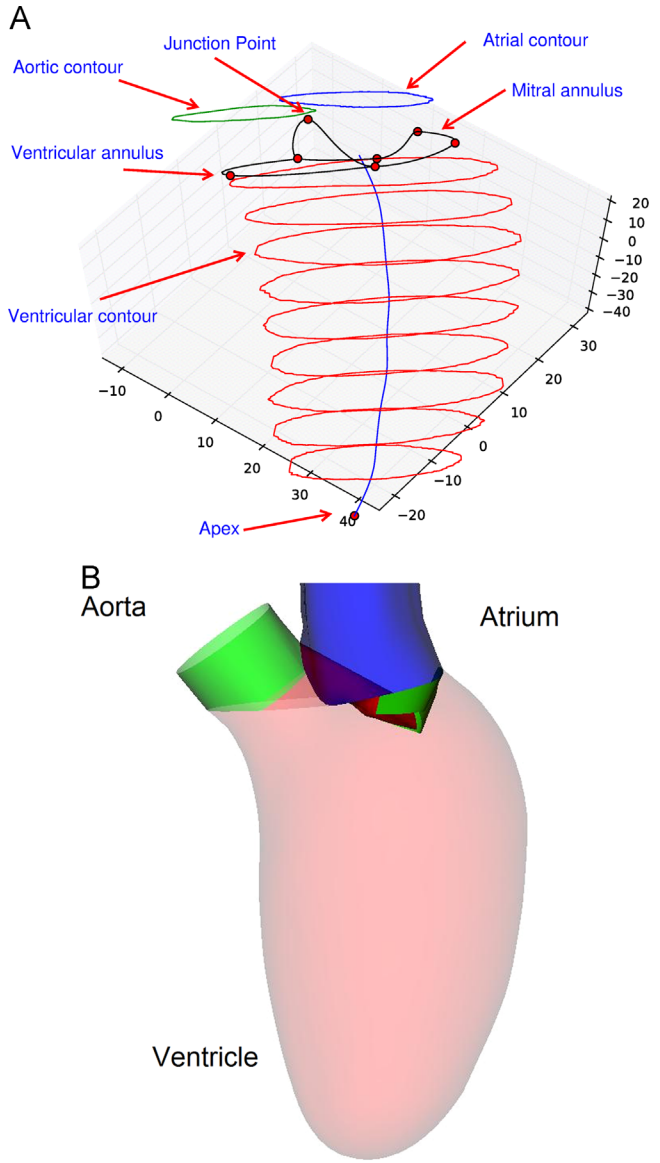

Fig. 2. LV reconstruction process from CMR images to CAD model. (A) Manual segmentation contours and points in 3D and (B) reconstructed LV model. (For interpretation of the references to color in this figure, the reader is referred to the web version of this article.)

in a similar manner. These two orifices partitioned the short-axis contours into three regions: atrium (blue), ventricle (red) and aorta (green). Circumferential and longitudinal interpolations were applied to improve the spatial resolution and smoothness, and the final Computer-Aided Design (CAD) model was illustrated in Fig. 2B.

Although the mitral leaflets crossed all long-axis images, they were only clearly visible in the three-chamber view image (Fig. 1). A pair of contours drawn along anterior and posterior leaflets was used for mitral valve reconstruction, and thus the information was inadequate to reconstruct a patient-specific mitral valve. As a result, equations were used to define the simplified MV geometries based on this pair of contours.

2.3. Posterior leaflet geometry

The mitral annulus was roughly circular in 3D, and it was assumed that its central axis was along the out-of-plane direction of short-axis view (Fig. 3). In the Cartesian system, a point on the mitral annulus can be written as:

$$x_{annulus} = x_{center} + r\ \sin\ \alpha\ \cos\ \theta$$

$$y_{annulus} = y_{center} + r\ \sin\ \alpha\ \sin\ \theta$$

$$z_{annulus} = z_{center} - r\ \cos\ \alpha \tag{1}$$

where $[x_{center}, y_{center}, z_{center}]$ are the coordinates of the center of mitral annulus; $r$is the distance between a point on annulus and the center; α is the angle between $r$and central axis; and θ is the angle between the projection (r sin α) and x axis. The cross section of posterior leaflet in the three-chamber view was a line segment with its root connected to the mitral annulus. Note that the cross section of posterior leaflet was assumed to be straight for the ease of definition. Therefore, the cross section of mitral leaflet on the plane defined by the central axis and a point on the mitral annulus could be represented by two points $[X_{annulus}, X_{tip}]$ (Fig. 3). The tip point can be expressed as:

$$x^p_{tip} = x^p_{annulus} + l\ \sin\ \beta\ \cos(\pi - \theta)$$

$$y^p_{tip} = y^p_{annulus} + l\ \sin\ \beta\ \sin(\pi - \theta)$$

$$z^p_{tip} = z^p_{annulus} - l\ \cos\ \beta \tag{2}$$

where l is the length of mitral leaflet; β is the angle between leaflet and the central axis and p denotes posterior. The posterior leaflet was assumed to be a semi truncated-cone shaped with respect to the central axis of mitral annulus. The maximum l was measured from the three-chamber view image, and it reduced gradually as the tip moved away from the three-chamber view plane (Fig. 3). The angle, β, was assumed to be constant for posterior leaflet.

2.4. Anterior leaflet geometry

During systole, the mitral valve was closed, and the edge of posterior leaflet could be employed to form the anterior leaflet. However, due to the limitation of CFD software, the fluid domain must be continuous, and a clearance gap was maintained between the posterior and anterior leaflets (Fig. 3). The anterior leaflet was also assumed to be semi-cylindrical as the posterior leaflet during diastole, and a tip can be expressed as:

$$x^a_{tip} = x^a_{annulus} + l\ \sin\ \varphi\ \cos\ \theta$$

$$y^a_{tip} = y^a_{annulus} + l\ \sin\ \varphi\ \sin\ \theta$$

$$z^a_{tip} = z^a_{annulus} - l\ \cos\ \varphi \tag{3}$$

where φ is the angle between the central axis and the cross section of anterior leaflet on the plane defined by central axis and a point on mitral annulus and $a$denotes anterior. The above mentioned procedure was programmed using Python programming language, and the CAD geometries were stored in STereo-Lithography (STL) format.

2.5. Numerical modeling

To model the blood flow in pumping LV, the finite volume method in arbitrary-Lagrangian Eulerian (ALE) formulation of the Navier–Stokes equations was employed. The integral forms of continuity and momentum equations are expressed as:

$$\frac{\partial}{\partial t}\int_V \rho dV + \int_S \rho\left(\vec{v} - \vec{v_b}\right)\cdot\vec{n}\,dS = 0 \tag{4}$$

$$\frac{\partial}{\partial t}\int_V \rho\vec{v}\,dV + \int_S \left(\rho\vec{v}\left(\vec{v} - \vec{v_b}\right) + pI - \vec{\tau}\right)\cdot\vec{n}\,dS = 0 \tag{5}$$

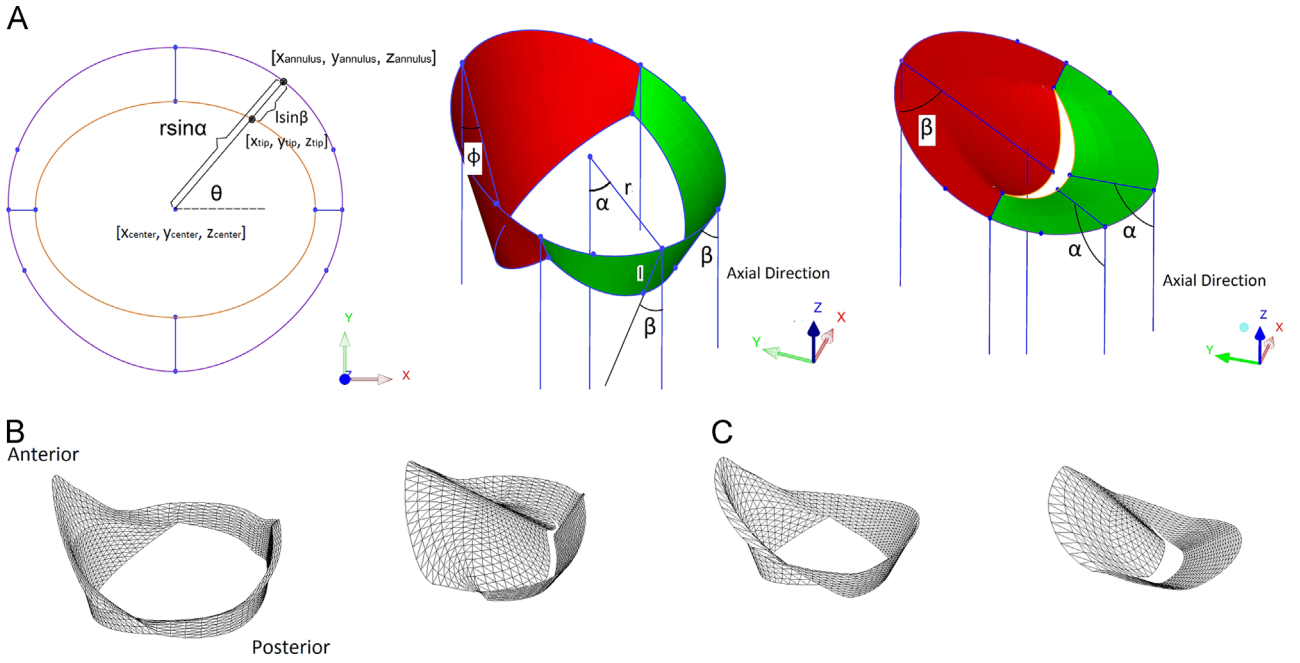

Fig. 3. MV model. (A) Ideal MV geometries in different views, (B) MV geometries in normal subject, and (C) MV geometries in PAH patient.

where ρ is the fluid density; $\vec{v}$ is the velocity vector of fluid; $\vec{v_b}$ is the velocity vector of moving boundary; $\vec{n}$ is the outwardly directed vector normal to dS; S is the boundary of the control volume, V; p is the pressure; I is the unit tensor; and $\vec{\tau}$ is the viscous stress tensor. Blood flow was assumed to be laminar and Newtonian with constant dynamic viscosity of 3.5 mPa s and density of 1050 kg/m^3 (Su et al., 2015). In this study, the CFD simulation was conducted using commercial software, FLUENT (Version 14.0 ANSYS). The numerical model was meshed using tetrahedral grids to cope with large deformation, and both spring-based smoothing and local remeshing algorithm embedded in dynamic mesh model were activated to avoid degradation of grid quality.

No-slip boundary condition was applied to ventricular wall and leaflets, and their motions were prescribed according to the CMR images. Cubic-spline interpolation was applied to increase the temporal resolution of CMR acquisition, and the deformation was implemented using user-defined function (UDF) (Su et al., 2014a). No mitral or aortic valve regurgitation was observed in these two cases, and thus the inlet and outlet were set to be wall (*i.e.* fully closed) during systole and diastole, respectively. Meanwhile, the boundary condition at the outlet during systole was pressure outlet, and that at inlet during diastole was pressure inlet. To model the unsteady blood flow, pressure-based solver was selected, and SIMPLEC scheme was adopted for the pressure–velocity coupling. The spatial discretizations of pressure and momentum were of second-order, while temporal discretization was only of first-order when dynamic mesh module was enabled.

3. Results

3.1. Global parameters of numerical models

Based on CMR images, the LV geometries in both cases were reconstructed as demonstrated in Fig. 4A. The normal LV was essentially elliptical and its cross section on the short-axis plane was circular. However, the PAH in the right heart considerably flattened the septum and remodeled the LV into D-shape in the

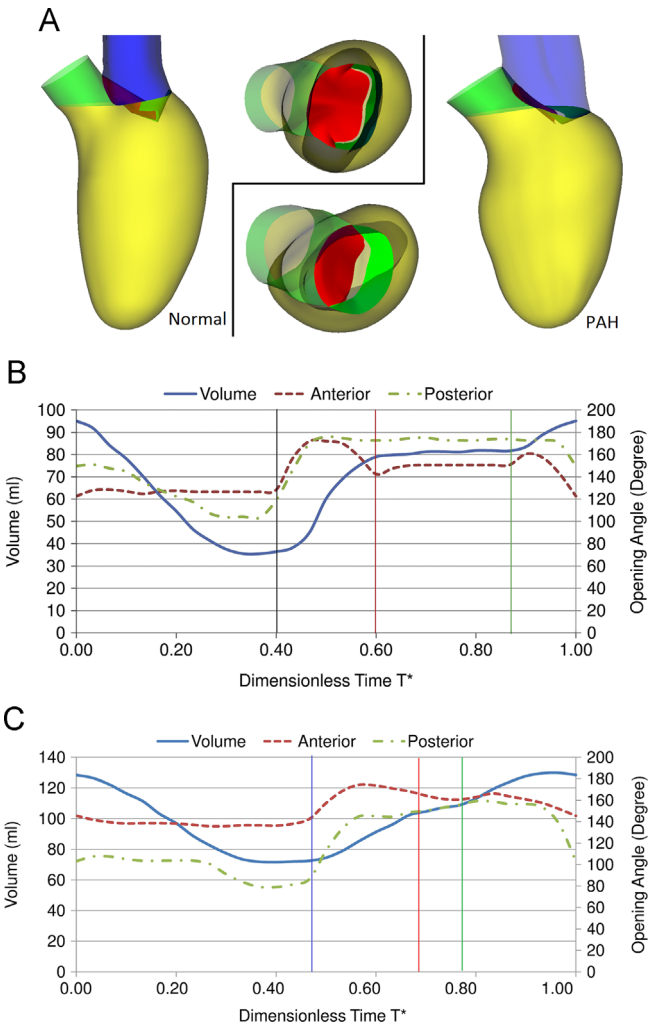

Fig. 4. LV and MV geometries reconstructed from CMR. (A) CAD models of LVs, (B) plots of ventricular volume and leaflet opening angles in normal subject, and (C) plots of ventricular volume and leaflet opening angles in PAH patient.

Please cite this article as: Su, B., et al., Cardiac MRI based numerical modeling of left ventricular fluid dynamics with mitral valve incorporated. Journal of Biomechanics (2016), http://dx.doi.org/10.1016/j.jbiomech.2016.03.008

short-axis view. The saddle-shaped mitral annulus tilted towards the septum, and the presence of asymmetric bileaflet mitral valve rectified the opening direction toward the apex regardless of the LV geometry. Based on the end-diastolic volume (EDV) and the end-systolic volume (ESV), the ejection fraction (EF = 1 − ESV/EDV) of the normal subject was 61.6%, and the systolic duration was 40% of the cardiac cycle. The PAH patient had a lower EF of 43.6% and a longer systolic duration of 46.6%. The diastasis duration in the normal subject was 26.7%, whereas that in the PAH patient was only 10%. In addition, the atrial contraction contributed to 23.2% of the stroke volume in the normal subject, while it was 35.2% in the PAH patient. Based on the definition of vortex formation time (VFT) (Gharib et al., 1998), which is a dimensionless parameter to quantify the duration of mitral jet into the LV, the values in normal subject and PAH patient were 4.0 and 6.5, respectively. Note that the normal VFT varies from 3.5 to 5.5 (Kheradvar et al., 2012). The parameters are listed in Table 1 for the ease of comparison.

Fig. 4B and C shows the LV volumetric variation and both anterior and posterior leaflet angles extracted. Although the cardiac cycle can be divided into a number of phases, it was simply classified into two phases: diastole and systole, according to the status of mitral valve. As shown in Fig. 4, these two phases are separated by a vertical line, where both leaflets start opening rapidly. As only the vortex structure developed during diastole was concerned in this study, the diastole was further divided into three sub-phases: rapid filling, diastasis and atrial contraction, based on the characteristics of volumetric variation curve. Although these three sub-phases could only be clearly identified in the normal subject (Fig. 4B), they were also applied to the PAH patient for the ease of comparison (Fig. 4C). Because no valvular diseases were present in both cases, the mitral valve opened rapidly at the onset of diastole. Based on the variation of opening angle of anterior leaflet, the partial closure phenomenon was present in the diastole. Near the end of diastole, the leaflets closed sharply. Although the mitral valve was fully closed without regurgitation during systolic phase, the opening angles were still varying, owing to the change of pressure difference between LV and atrium and the motion of mitral annulus.

Table 1
Parameters obtained from LV and MV geometries. EDV: End of Diastolic Volume; ESV: End of Systolic Volume; SV: Stroke Volume; EF: Ejection Fraction; ACV: Atrial Contraction Volume; DD: Duration of Diastasis; VFT: Vortex Formation Time.

Subject	EDV ml	ESV ml	SV ml	EF %	ACV %	DD %	VFT
Normal	95.1	36.5	58.6	61.6	23.2	26.7	4.0
PAH	128.4	72.4	56.0	43.6	35.2	10.0	6.5

3.2. Vortex structures of diastolic flow

Fig. 5 shows the vortex structures of diastolic flow in the normal subject at five characteristic instants. Near the onset of rapid filling phase, a vortex ring formation and pinch-off were observed at the mitral valve tip (Fig. 5a and b). The vortex ring propagated towards the apex and interacted with the ventricular flow. Therefore, the vortex ring was disrupted and only scattered eddies were observed during the diastasis (Fig. 5c). Similarly, another vortex ring was developed during the atrial contraction phase (Fig. 5d). Because the LV was considerably dilated compared with that during the rapid filling phase, the vortex ring did not interact with the ventricular flow, and the short duration of atrial contraction phase did not allow this vortex ring to penetrate further into LV chamber before it was washed out of LV (Fig. 5e).

Fig. 6 shows the vortex structures in the PAH patients. Initially, a vortex ring formed at the mitral leaflet tips and a smaller secondary structure was also observed after the primary vortex ring pinch-off (Fig. 6a and b). Due to PAH, the septum bulged towards the LV (as shown in Fig. 4A), and disrupted the vortex ring. In contrast, the other portion of the LV except the septum was more dilated along radial direction (*e.g.* posterior wall), and the corresponding part of the vortex ring did not impinge on the LV. As a result, it was preserved until the end of rapid filling phase. The longer duration of atrial contraction phase allowed the newly formed vortex ring to develop and penetrate further down, though the ring was partially broken by the septum (Fig. 6d and e). Besides eddies induced during the atrial contraction phase, those initiated in the rapid filling phase did not dissipate completely, because the end-diastolic volume of PAH patient was larger than that of normal subject (Fig. 6e).

4. Discussion

Most of the numerical simulations focused on the normal subjects, and only a few types of myocardial diseases were investigated in the literature. To the best of our knowledge, this study was the first attempt to model LV in a PAH patient using patient-specific CMR images. In addition, the MV was incorporated in the numerical model, which was mostly neglected in other studies. Although Dimasi et al. (2012) reconstructed the LV, MV and aorta based on CMR images, they only investigated the flow field during systolic phase (*i.e.* the MV was fully closed). In addition to exhibiting a shortening motion in longitudinal direction, the saddle-shaped mitral annulus experiences sphincter contraction, which could vary the annular area by approximately 25% (Silbiger and Bazaz, 2009). Therefore, the simplification of mitral annulus as a rigid circular orifice (Domenichini and Pedrizzetti, 2014; Seo et al., 2014) could underestimate the strength of

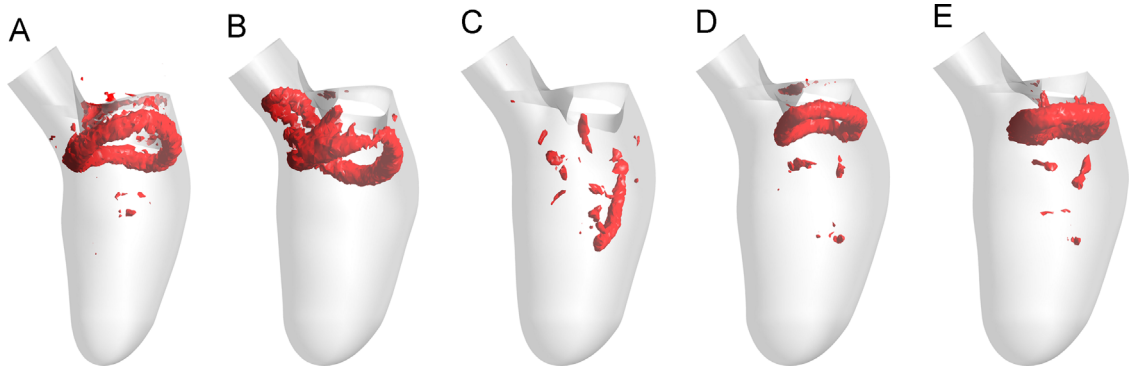

Fig. 5. 3D vortex structure visualized by iso-surface of Q-criterion vortex identification during diastole in the normal subject. From (A) to (E): t/T = [0.5, 0.57, 0.8, 0.93, 0.96].

Please cite this article as: Su, B., et al., Cardiac MRI based numerical modeling of left ventricular fluid dynamics with mitral valve incorporated. Journal of Biomechanics (2016), http://dx.doi.org/10.1016/j.jbiomech.2016.03.008

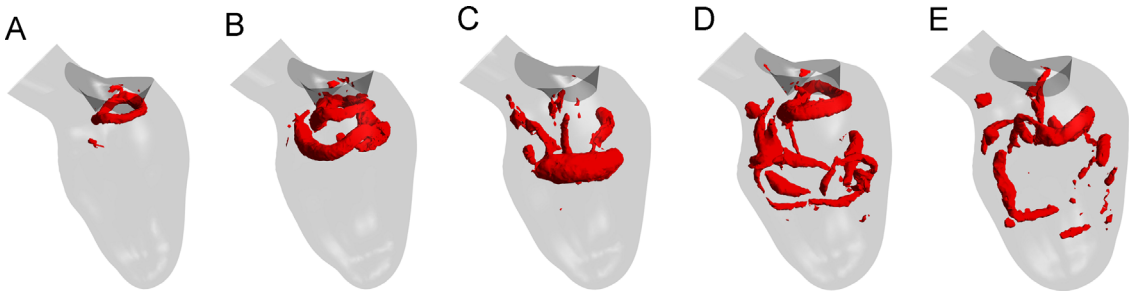

Fig. 6. 3D vortex structure visualized by iso-surface of Q-criterion vortex identification during diastole in the PAH patient. From (A) to (E): t/T=[0.53, 0.63, 0.73, 0.83, 0.93].

transmitral jet to some extent. Despite the detailed geometry of MV, its presence reduces the effective opening area and alters the VFT (Kheradvar et al., 2012). In the numerical models ignoring the MV, VFT in a normal subject was only about 2 (Le and Sotiropoulos, 2012; Nguyen et al., 2013). Furthermore, in *in-vivo* studies using 2D Echocardiography, the VFTs in the normal subject were around 1.63 in (Stewart et al., 2012) and 2.67 in (Poh et al., 2012), which were similar to the numerical model without MV. It was because the diameter of mitral annulus instead of effective diameter of mitral geometric orifice area (Kheradvar et al., 2012) was applied to calculate VFT. In other words, these *in-vivo* measurements did not consider the effect of mitral leaflet on the mitral opening area. In this study, the VFT was calculated from the CMR-based four-dimensional LV geometry and effective opening area of MV, which overcame the limitations of 2D echocardiography as mentioned by Belohlavek (2012). Therefore, the VFT of 4 in the healthy volunteer was within the normal range of 3.5–5.5 as anticipated in the theoretical analysis and experimental visualization (Gharib et al., 1998). In contrast, the VFT of the PAH patient was 6.5, due to reduced MV opening area induced by the hypertension in right ventricle. Therefore, this study demonstrated that VFT is a promising parameter to assess the diastolic function of LV.

In most numerical simulations of LV flow, the mitral annulus was assumed to be perpendicular to the apex in order to deliberately direct the LV flow in the clockwise direction (Krittian et al., 2010; Le and Sotiropoulos, 2012; Pedrizzetti and Domenichini, 2007; Seo et al., 2014; Su et al., 2015). However, the mitral annulus tilts towards the septum, which is expected to result in counter-clockwise flow direction, which is evidenced by the observation in an *in-vivo* study (Pedrizzetti et al., 2010) and numerical study (Schenkel et al., 2009). The much longer anterior leaflet redirects the transmitral jet towards the apex, enhancing the dominant clockwise flow pattern in LV. Furthermore, the presence of MV is expected to decrease the sensitivity of LV flow to the atrium, since the transmitral flow is mainly affected by MV. It is widely accepted that the MV leaflets have significant influences on the formation and development of vortex ring that is the dominant feature of LV flow (Charonko et al., 2013; Mihalef et al., 2011; Su et al., 2014b). In the literature, comparisons between 2D model with MV (Su et al., 2014b) and that without MV (Khalafvand et al., 2012) demonstrated the difference in the mechanism of vortex formation. The anterior vortex in the valveless model was initiated by large divergence curvature at the junction of the mitral and aortic root, while that in the model with MV resulted from flow separation at the leaflet tip, which was observed in Figs. 5 and 6. Moreover, the 3D models showed that MV leaflets promoted the penetration of vortex ring, leading to better mixing and washout of apical flow (Seo and Mittal, 2013; Seo et al., 2014). The longer anterior leaflet was immersed in the core region of LV, and it was more susceptible to the intraventricular flow than the shorter posterior leaflet. Therefore, the development of the anterior vortex partially swayed the anterior leaflet inward, which was evidenced by the leafleted opening angle decreasing after the rapid filling phase in Fig. 4. This partial closure phenomenon was obvious in anterior leaflet regardless of the status of LV.

Based on the comparison with the normal subject, it can be observed that PAH considerably distorted the LV geometry and the flattened septum disrupted the vortex ring. The dilated LV had large radial space except the septum, so the vortex structure dissipated its energy more slowly than that in the normal subject. As a result, the vortex ring was largely preserved during the diastasis in PAH as demonstrated in Figs. 5 and 6. At the onset of rapid filling, the trailing flow structure behind the primary vortex ring was observed only in PAH. It was due to the excessive VFT, and this phenomenon was also observed in other studies (Gharib et al., 1998; Zheng et al., 2012).

Owing to the relatively low image acquisition rate of CMR, the leaflet dynamics during the opening and closing phases had to be interpolated temporally, which was the main limitation of this study. In the latest study conducted by Domenichini and Pedrizzetti (2014), the simplified one degree of freedom (*i.e.* the angle of mitral leaflet opening angle) was introduced to couple the intraventricular flow and leaflet dynamics. The routine CMR images included two-chamber, three-chamber and four-chamber views along long-axis, and therefore the saddle-shaped mitral annulus was reconstructed using only six points, which either overestimated or underestimated the true mitral orifice area. Due to the difficulty in reconstructing mitral valve based on long-axis images, the leaflets in the current study were slightly shorter, and thus the coaptation zone was ignored. Only two cases were modeled in this study, and a larger sample size is necessary to demonstrate the effects of PAH on intraventricular flow.

5. Conclusion

This study was the first attempt to simulate the flow in LV with MV incorporated based on CMR, which is more widely used for patients with myocardial diseases than CT. Based on the geometries and opening area of mitral valve, the resultant VFTs in the normal subject and the PAH patient varies significant, which is consistent with the observations in the literature. Therefore, VFT is a promising parameter to differentiate normal and diseased LVs. The detailed vortex structures showed that the MV played an important role in the generation of vortex ring, and the asymmetric bileaflet MV directed the transmitral jet towards the apex. Although the MV was based only on the mitral annulus and two segments in three-chamber view, it resulted in a more realistic flow field than the valveless model in the literature. With further improvements in modeling leaflet dynamics, the framework developed in this study can be applied to various patient-specific LV simulations.

Please cite this article as: Su, B., et al., Cardiac MRI based numerical modeling of left ventricular fluid dynamics with mitral valve incorporated. Journal of Biomechanics (2016), http://dx.doi.org/10.1016/j.jbiomech.2016.03.008

Conflict of interest statement

The authors declare that they have no conflict of interest in regards to this study.

Acknowledgment

The authors would like to acknowledge Goh Cardiovascular Research Award (Duke-NUSGCR/2013/0009) for funding this research.

References

Belohlavek, M., 2012. Vortex formation time: an emerging echocardiographic index of left ventricular filling efficiency? Eur. Heart J. Cardiovasc. Imaging 13, 367–369.

Chandran, K.B., Kim, H., 2014. Computational mitral valve evaluation and potential clinical applications. Ann. Biomed. Eng.

Charonko, J.J., Kumar, R., Stewart, K., Little, W.C., Vlachos, P.P., 2013. Vortices formed on the mitral valve tips aid normal left ventricular filling. Ann. Biomed. Eng. 41, 1049–1061.

Chnafa, C., Mendez, S., Nicoud, F., 2012. Image-based patient-specific simulation: a computational modelling of the human left heart haemodynamics. Comput. Methods Biomech. Biomed. Eng. 15, 1–3.

Chnafa, C., Mendez, S., Nicoud, F., 2014. Image-based large-eddy simulation in a realistic left heart. Comput. Fluids 94, 173–187.

Dimasi, A., Cattarinuzzi, E., Stevanella, M., Conti, C.A., Votta, E., Maffessanti, F., Ingels, N.B., Redaelli, A., 2012. Influence of mitral valve anterior leaflet in vivo shape on left ventricular ejection. Cardiovasc. Eng. Technol. 3, 388–401.

Domenichini, F., Pedrizzetti, G., 2014. Asymptotic model of fluid–tissue interaction for mitral valve dynamics. Cardiovasc. Eng. Technol. 6, 95–104.

Falahatpisheh, A., Kheradvar, A., 2012. High-speed particle image velocimetry to assess cardiac fluid dynamics in vitro: from performance to validation. Eur. J. Mech. - B/Fluids 35, 2–8.

Garcia, D., Del Alamo, J.C., Tanne, D., Yotti, R., Cortina, C., Bertrand, E., Antoranz, J.C., Perez-David, E., Rieu, R., Fernandez-Aviles, F., Bermejo, J., 2010. Two-dimensional intraventricular flow mapping by digital processing conventional color-doppler echocardiography images. IEEE Trans. Med. Imaging 29, 1701–1713.

Gharib, M., Rambod, E., Shariff, K., 1998. A universal time scale for vortex ring formation. J. Fluid Mech. 360, 121–140.

Khalafvand, S.S., Ng, E.Y.K., Zhong, L., Hung, T.K., 2012. Fluid-dynamics modelling of the human left ventricle with dynamic mesh for normal and myocardial infarction: preliminary study. Comput. Biol. Med. 42, 863–870.

Khalafvand, S.S., Zhong, L., Ng, E.Y.K., 2014. Three-dimensional CFD/MRI modeling reveals that ventricular surgical restoration improves ventricular function by modifying intraventricular blood flow. Int. J. Numer. Methods Biomed. Eng. 30, 1044–1056.

Kheradvar, A., Assadi, R., Falahatpisheh, A., Sengupta, P.P., 2012. Assessment of transmitral vortex formation in patients with diastolic dysfunction. J. Am. Soc. Echocardiogr. 25, 220–227.

Kheradvar, A., Gharib, M., 2007. Influence of ventricular pressure drop on mitral annulus dynamics through the process of vortex ring formation. Ann. Biomed. Eng. 35, 2050–2064.

Krittian, S., Schenkel, T., Janoske, U., Oertel, H., 2010. Partitioned fluid-solid coupling for cardiovascular blood flow: validation study of pressure-driven fluid-domain deformation. Ann. Biomed. Eng. 38, 2676–2689.

Le, T.B., Sotiropoulos, F., 2012. On the three-dimensional vortical structure of early diastolic flow in a patient-specific left ventricle. Eur. J. Mech. B. Fluids 35, 20–24.

Mangual, J.O., Kraigher-Krainer, E., De Luca, A., Toncelli, L., Shah, A., Solomon, S., Galanti, G., Domenichini, F., Pedrizzetti, G., 2013. Comparative numerical study on left ventricular fluid dynamics after dilated cardiomyopathy. J. Biomech. 46, 1611–1617.

Mihalef, V., Ionasec, R.I., Sharma, P., Georgescu, B., Voigt, I., Suehling, M., Comaniciu, D., 2011. Patient-specific modelling of whole heart anatomy, dynamics and haemodynamics from four-dimensional cardiac CT images. Interface Focus 1, 286–296.

Nguyen, V.-T., Loon, C.J., Nguyen, H.H., Liang, Z., Leo, H.L., 2013. A semi-automated method for patient-specific computational flow modelling of left ventricles. Comput. Methods Biomech. Biomed. Eng., 37–41.

Pedrizzetti, G., Domenichini, F., 2007. Asymmetric opening of a simple bileaflet valve. Phys. Rev. Lett. 98, 214503.

Pedrizzetti, G., Domenichini, F., 2014. Left ventricular fluid mechanics: the long way from theoretical models to clinical applications. Ann. Biomed. Eng. 43, 26–40.

Pedrizzetti, G., Domenichini, F., Tonti, G., 2010. On the left ventricular vortex reversal after mitral valve replacement. Ann. Biomed. Eng. 38, 769–773.

Poh, K.K., Lee, L.C., Shen, L., Chong, E., Tan, Y.L., Chai, P., Yeo, T.C., Wood, M.J., 2012. Left ventricular fluid dynamics in heart failure: echocardiographic measurement and utilities of vortex formation time. Eur. Heart J. Cardiovasc. Imaging 13, 385–393.

Rodriguez Muñoz, D., Markl, M., Moya Mur, J.L., Barker, A., Fernández-Golfín, C., Lancellotti, P., Zamorano Gómez, J.L., 2013. Intracardiac flow visualization: current status and future directions. Eur. Heart J. Cardiovasc. Imaging 14, 1029–1038.

Saber, N.R., Wood, N.B., Gosman, a D., Merrifield, R.D., Yang, G.-Z., Charrier, C.L., Gatehouse, P.D., Firmin, D.N., 2003. Progress towards patient-specific computational flow modeling of the left heart via combination of magnetic resonance imaging with computational fluid dynamics. Ann. Biomed. Eng. 31, 42–52.

Schenkel, T., Malve, M., Reik, M., Markl, M., Jung, B., Oertel, H., 2009. MRI-based CFD analysis of flow in a human left ventricle: methodology and application to a healthy heart. Ann. Biomed. Eng. 37, 503–515.

Seo, J.H., Mittal, R., 2013. Effect of diastolic flow patterns on the function of the left ventricle. Phys. Fluids 25, 110801.

Seo, J.H., Vedula, V., Abraham, T., Lardo, A.C., Dawoud, F., Luo, H., Mittal, R., 2014. Effect of the mitral valve on diastolic flow patterns. Phys. Fluids 26, 121901.

Silbiger, J.J., Bazaz, R., 2009. Contemporary insights into the functional anatomy of the mitral valve. Am. Heart J. 158, 887–895.

Stevanella, M., Maffessanti, F., Conti, C. a, Votta, E., Arnoldi, A., Lombardi, M., Parodi, O., Caiani, E.G., Redaelli, A., 2011. Mitral valve patient-specific finite element modeling from cardiac MRI: application to an annuloplasty procedure. Cardiovasc. Eng. Technol. 2, 66–76.

Stewart, K.C., Charonko, J.C., Niebel, C.L., Little, W.C., Vlachos, P.P., 2012. Left ventricle filling vortex formation is unaffected by diastolic impairment. Am. J. Physiol.: Heart Circ. Physiol., 1255–1262.

Su, B., Kabinejadian, F., Phang, H.Q., Kumar, G.P., Cui, F., Kim, S., Tan, R.S., Hon, J.K.F., Allen, J.C., Leo, H.L., Zhong, L., 2015. Numerical modeling of intraventricular flow during diastole after implantation of BMHV. PLoS One 10, e0126315.

Su, B., Zhang, J.-M., Tang, H.C., Wan, M., Lim, C.C.W., Su, Y., Zhao, X., Tan, R.S., Zhong, L., 2014a. Patient-specific blood flows and vortex formations in patients with hypertrophic cardiomyopathy using computational fluid dynamics. In: Proceedings of IEEE Conference on Biomedical Engineering and Sciences (IECBES) 2014.

Su, B., Zhong, L., Wang, X.-K., Zhang, J.-M., Tan, R.S., Allen, J.C., Tan, S.K., Kim, S., Leo, H.L., 2014b. Numerical simulation of patient-specific left ventricular model with both mitral and aortic valves by FSI approach. Comput. Methods Programs Biomed. 113, 474–482.

Votta, E., Le, T.B., Stevanella, M., Fusini, L., Caiani, E.G., Redaelli, A., Sotiropoulos, F., 2013. Toward patient-specific simulations of cardiac valves: state-of-the-art and future directions. J. Biomech. 46, 217–228.

Zheng, X., Seo, J.H., Vedula, V., Abraham, T., Mittal, R., 2012. Computational modeling and analysis of intracardiac flows in simple models of the left ventricle. Eur. J. Mech. - B/Fluids 35, 31–39.

Please cite this article as: Su, B., et al., Cardiac MRI based numerical modeling of left ventricular fluid dynamics with mitral valve incorporated. Journal of Biomechanics (2016), http://dx.doi.org/10.1016/j.jbiomech.2016.03.008